9-21-2018

Discontinuous Phase Transitions in Nonlocal Schloegl Models for Autocatalysis: Loss and Reemergence of a Nonequilibrium Gibbs Phase Rule

Da-Jiang Liu
Ames Laboratory

Chi-Jen Wang
National Chung Cheng University

James W. Evans
Iowa State University and Ames Laboratory, jevans@ameslab.gov

Discontinuous Phase Transitions in Nonlocal Schloegl Models for Autocatalysis: Loss and Reemergence of a Nonequilibrium Gibbs Phase Rule

Abstract
We consider Schloegl models (or contact processes) where particles on a square grid annihilate at a rate p and are created at a rate of $k_n=n(n-1)/[N(N-1)]$ at empty sites with n particles in a neighborhood ΩN of size N. Simulation reveals a discontinuous transition between populated and vacuum states, but equistable $p=p_{eq}$ determined by the stationarity of planar interfaces between these states depends on the interface orientation and on ΩN. The behavior for large ΩN follows from continuum equations. These also depend on the interface orientation and on ΩN shape, but a unique $p_{eq}=0.211\ 376\ 320\ 4$ emerges imposing a Gibbs phase rule.

Disciplines
Elementary Particles and Fields and String Theory

Discontinuous Phase Transitions in Nonlocal Schloegl Models for Autocatalysis: Loss and Reemergence of a Nonequilibrium Gibbs Phase Rule

Da-Jiang Liu,[1] Chi-Jen Wang,[2] and James W. Evans[1,3,4]
[1]Ames Laboratory—USDOE, Iowa State University, Ames, Iowa 50011, USA
[2]Department of Mathematics, National Chung Cheng University, Chiayi 62102, Taiwan
[3]Department of Mathematics, Iowa State University, Ames, Iowa 50011, USA
[4]Department of Physics and Astronomy, Iowa State University, Ames, Iowa 50011, USA

(Received 5 April 2018; revised manuscript received 25 July 2018; published 21 September 2018)

We consider Schloegl models (or contact processes) where particles on a square grid annihilate at a rate p and are created at a rate of $k_n = n(n-1)/[N(N-1)]$ at empty sites with n particles in a neighborhood Ω_N of size N. Simulation reveals a discontinuous transition between populated and vacuum states, but equistable $p = p_{eq}$ determined by the stationarity of planar interfaces between these states depends on the interface orientation and on Ω_N. The behavior for large Ω_N follows from continuum equations. These also depend on the interface orientation and on Ω_N shape, but a unique $p_{eq} = 0.211\,376\,320\,4$ emerges imposing a Gibbs phase rule.

DOI: 10.1103/PhysRevLett.121.120603

Basic open questions remain regarding phase transitions between steady states in statistical mechanical models of nonequilibrium systems where a free-energy framework is not available to aid analysis [1–5]. For discontinuous transitions with a single control parameter p, the Gibbs phase rule in equilibrium systems requires that these transitions occur at a unique $p = p_{eq}$ where the two phases coexist with equal chemical potentials [6]. For nonequilibrium systems, phase coexistence or equistability is usually determined by stationarity of a planar interface separating the two phases [7,8], a criterion also applicable to equilibrium systems. However, for nonequilibrium systems, phase coexistence can occur over a finite range of the control parameter p (so-called generic two-phase coexistence, 2PC) [9–14]. This feature can be manifested by a dependence of p_{eq} on the interface orientation. In a regime of generic 2PC, both states are in some sense stable against perturbation by the other state. Such a behavior is manifested, e.g., in Toom's model [9–11], pinned interface models [12], and certain contact processes [13,14]. In addition to elucidating poorly understood generic 2PC, related challenges remain for the characterization of metastability and associated nucleation phenomena [15–18].

To advance fundamental understanding of these issues, it is desirable to construct suitable single-component stochastic lattice-gas models with simple "symmetric rules" (avoiding an asymmetry in Toom's rules and the complexity of heterogeneous interface pinning models or of multicomponent models). Furthermore, the models are naturally constructed to exhibit mean-field (MF) bistability of steady states. MF bistability is a ubiquitous phenomenon in both equilibrium systems (e.g., van der Waals equation of state) and in diverse nonequilibrium systems (describing catalysis, spatial epidemics, population dynamics, etc.) [19,20]. It can signal the presence of a discontinuous transition in the stochastic model where fluctuations and correlations generally preclude exact analysis. We will explore a suitably crafted class of models motivated by Schloegl's second model for autocatalysis [13,14,17,20–24] where particles reside at the sites of a square lattice. Particles spontaneously annihilate at rate p and are created autocatalytically at empty sites if there are $n \geq 2$ particles within a prescribed neighborhood of that site. These models are equivalent to spatial contact processes with threshold 2 describing the spread of epidemics [13,14,25–31]. In this application, empty (filled) sites in the Schloegl model are reassigned as healthy (infected) sites. Then, infected sites recover at rate p, and healthy sites can become infected given two or more nearby infected individuals. Such contact processes are also adopted to describe, e.g., the spread of information.

Often, the neighborhood influencing particle creation (or infection) includes just four nearest-neighbor (NN) sites on the square lattice. Studies of these models revealed a discontinuous phase transition exhibiting generic 2PC [13,14,17]. However, this is not broadly recognized or accepted [30,31], perhaps since a prominent study by Grassberger [22] of one realization of Schloegl's second model revealed a continuous transition (but this does not imply the same is true of other realizations). Here, we allow the possibility of general neighborhoods Ω_N of N sites and judiciously select creation rates

$$k_n = \frac{\binom{N-2}{n-2}}{\binom{N}{n}} = \frac{\binom{n}{2}}{\binom{N}{2}} = \frac{n(n-1)}{N(N-1)}$$

to ensure that all models share the same MF kinetics (see below). Our extension to general "nonlocal" neighborhoods reflects a strategy used for elucidation of critical phenomena in equilibrium [32,33] and nonequilibrium [34,35] models and connects with classic nonlocal continuum contact processes for epidemic or information spread with long-range infection or communication [36]. Furthermore, the construction of this general class of models allows us to address a postulate by Grinstein and co-workers [37] that model discreteness is not intrinsic to generic 2PC; i.e., if a discrete model incorporates features inducing generic 2PC, then the same should hold for the analogous continuum model. We find that this is not the case for our models.

In this Letter, first for our new appropriately crafted class of nonlocal Schloegl models, we develop an exact master-equation-based formulation describing model behavior importantly including heterogeneous states. Next, we present results from suitably tailored kinetic Monte Carlo (KMC) simulations within a constant-concentration ensemble precisely assessing model behavior both for small Ω_N where 2PC is revealed and for large Ω_N where surprisingly a unique and universal $p_{\rm eq}$ emerges. For a deeper understanding of the latter, we provide an analytic treatment of interface propagation for large Ω_N in terms of continuum integrodifferential equations (IDEs) which are rigorously derived from the above exact heterogeneous master equations. While stationary front solutions for continuum reaction-diffusion equations (RDEs) can often be analyzed by direct mapping onto a Hamiltonian problem [20], this is not the case for IDEs. Nonetheless, exact analysis of the IDE is achieved by mapping onto an infinite-dimensional dissipative dynamical system. This integrated combination of tailored KMC simulation and novel analytic analysis enables a significant advance in the current limited understanding of subtle generic 2PC phenomena and of the applicability or otherwise of Gibbs-type phase rules for nonequilibrium systems.

For spatially homogeneous states, the overall fraction or concentration $C = C(t)$ of populated sites in our models satisfies

$$d/dt\, C \equiv R(C,p) = -pC + K_{\rm tot}, \tag{1}$$

with total particle creation rate per site $K_{\rm tot} = \sum_{2\le n\le N} k_n P_n (1-C)$. Here, P_n is the probability of exactly n populated sites in Ω_N which reflects nontrivial spatial correlations. If p is not too large, there will exist a populated steady state with $C = C_{\rm act}(p) > 0$, and $C(t) \to C_{\rm act}(p)$ for sufficiently high $C(0)$. One finds that $C_{\rm act}(p) \approx 1\text{-}p$ as $p \to 0$, since $K_{\rm tot}(p) \approx k_N(1\text{-}p) = 1\text{-}p$. For sufficiently large p, annihilation overwhelms particle creation and $C(t) \to C_{\rm vac}(p) \equiv 0$, the absorbing vacuum steady state. This absorbing state exists for all $p > 0$. Finally, we note that a MF treatment neglecting spatial correlations in site population implies that $P_n = \binom{N}{n} C^n (1-C)^{N-n}$. Consequently, the MF $K_{\rm tot}$ and $R(C,p)$ are independent of Ω_N and given by

$$K_{\rm tot}({\rm MF}) = (1-C)C^2 \quad \text{and}$$
$$R_{\rm MF}(C,p) = -pC + (1-C)C^2. \tag{2}$$

The MF steady states are given by $C_\pm(p) = \frac{1}{2} \pm \frac{1}{2}(1-4p)^{1/2}$ for $0 \le p \le \frac{1}{4}$ and $C = 0$ (the vacuum). C_+ corresponds to the stable populated state and C_- to an unstable state. As an aside, we remark that the same MF kinetics applies for Durrett's $N = 4$ model where Ω_4 includes NN sites and creation rates satisfy $k = m/4$ where m is the number of diagonal NN populated pairs in Ω_4 [13,25].

Analysis of spatially heterogeneous states, and specifically, the propagation of interfaces between populated and vacuum steady states, is central to the assessment of equistability. Thus, we develop an exact heterogeneous version [24,38,39] of Eq. (1). Let $C_{i,j} = P[x_{i,j}]$ denote the ensemble-averaged probability that site (i, j) is occupied (x), and $P[o_{i,j}]$ the probability that site (i, j) is empty (o) so that $P[x_{i,j}] + P[o_{i,j}] = 1$. Also, let $P[o_{i,j} - x_{k,l} - x_{m,n}]$ denote the probability that (i, j) is empty and both (k, l) and (m, n) are occupied, etc. Then, one has that

$$d/dt\, C_{i,j} = -pC_{i,j} + K_{\rm tot}(i,j), \tag{3}$$

where $K_{\rm tot}(i,j)$ denotes the total rate of particle creation at site (i, j). $K_{\rm tot}(i,j)$ involves a sum over contributions for each possible configuration of the neighborhood $\Omega_N(i,j)$ of empty site (i, j) with $n \ge 2$ populated sites associated with rate

$$k_n = \frac{\binom{n}{2}}{\binom{N}{2}}.$$

Each such contribution can be partitioned into $\binom{n}{2}$ equal contributions of $1/\binom{N}{2}$ times the relevant configuration probability for each of the $\binom{n}{2}$ pairs of populated sites. Combining all contributions associated with a specific populated pair, $K_{\rm tot}(i,j)$ reduces exactly to a sum over three-site probabilities with (i, j) empty and the specific pair populated,

$$K_{\rm tot}(i,j) = \sum_{(i',j')(i''',j''')\in\Omega_N} P[o_{i,j} - x_{i+i',j+j'} - x_{i+i'',j+j''}] \Big/ \binom{N}{2}. \tag{4}$$

The sum has $\binom{N}{2}$ terms avoiding double-counting pairs of sites in Ω_N. This exact reduction from $(N+1)$-site to three-site probabilities follows from our special choice of k_n. Applying Eq. (4) for uniform states immediately recovers

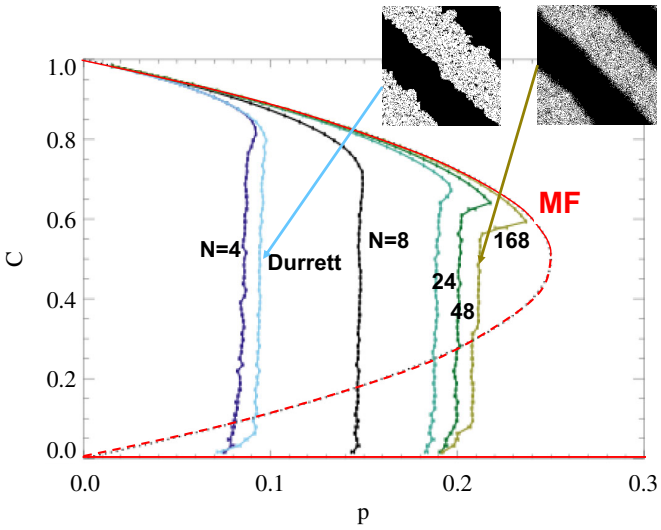

FIG. 1. Steady-state C versus p for square Ω_N for $N = L^2 - 1$ with $L \geq 3$ and for $N = 4$ from KMC simulations; $C = 0$ above the transition. The MF behavior is also shown. Inset: $S = 1$ strip geometries for $N = 4$, 128.

the MF result (2) after factorizing the three-site probability. More significantly, Eq. (4) will facilitate analytic treatment of behavior for large Ω_N, as described below.

Next, we assess the model behavior from KMC simulation. For discontinuous transitions, constant-concentration (CC) simulation [13,40,41] is particularly efficient. One selects a target concentration C_t, and by default initially populates sites randomly with $C \approx C_t$. Then, one picks a site at random and attempts to create (annihilate) a particle at that site if the current concentration satisfies $C < C_t$ ($C \geq C_t$). Tracking relative creation and annihilation rates produces a $p = p_t$ corresponding to $C = C_t$. The KMC results for steady-state $C(p)$ versus p are shown in Fig. 1, mainly for square Ω_N. A discontinuous transition at $p = p_{\rm eq}(N)$ occurs for all Ω_N, where $p_{\rm eq}(N) \approx p_{\rm eq}(\infty) - c/N$, for large N, for both the square and circular Ω_N, and where $p_{\rm eq}(\infty) \approx 0.2113(1)$ appears independent of neighborhood shape. See Fig. 2. Simulated configurations for $C_t \approx 0.5$ directly reveal phase separation. Convergence to MF behavior is evident for large N, as elucidated below.

Refinement to the above basic CC simulation analysis is needed to assess any orientation dependence of equistability. Here, one starts with a strip of populated sites with selected orientation or slope S, which is preserved provided the simulation maintains a strip geometry. See Fig. 1 (inset). The results of such simulations reveal an unambiguous variation of $p_{\rm eq}(S)$ with S for $N = 4$ with NN sites (a distance $r = a$ from the empty site for lattice constant a), $N = 8$ with 4NN sites ($r = \sqrt{5}a$), $N = 8$ with NN and 3NN sites ($r = a$, $2a$), and $N = 12$ (with $r = a$, $2a$, $3a$). See Table I. For $N = 8$ with NN and 2NN sites ($r = a$, $\sqrt{2}a$) and for $N > 8$, it is difficult to quantify any weak S dependence of $p_{\rm eq}(S)$, although this dependence plausibly

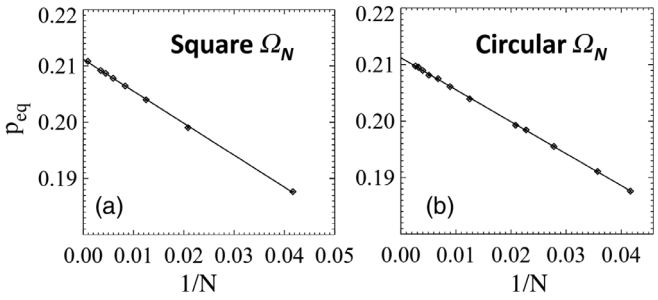

FIG. 2. $p_{\rm eq}(N)$ for (a) square and (b) circular Ω_N.

persists. In the simulations of Fig. 1 with random initial conditions, $p_{\rm eq}$ reflects an average over S of $p_{\rm eq}(S)$.

Henceforth, we focus on providing insight into the limiting behavior for large compact neighborhoods as $N \to \infty$. The distribution P_n of the number n of populated sites within Ω_N becomes narrowly distributed about the mean $n = NC$ so that $K_{\rm tot} = \sum_{2 \leq n \leq N} k_n P_n (1\text{-}C) \approx k_{n=\rm NC}(1\text{-}C) \to (1\text{-}C)C^2$ as $N \to \infty$, explaining the recovery of MF kinetics. However, our focus is on heterogeneous states. Thus, we consider a coarse-grained spatially continuous description of the concentration $C(\boldsymbol{x}, t) = C_{i,j}$, where $\boldsymbol{x} = (x, y) = (ia, ja)$. Since sites (i, j), $(i + i', j + j')$, and $(i + i'', j + j'')$ appearing in the sum in Eq. (4) are typically far separated, the correlations between the occupancies of these sites should be negligible. Then, factorizing three-site probabilities and converting Eq. (3) to coarse-grained continuum notation yields

$$\partial/\partial t\, C(\boldsymbol{x}, t) = -pC(\boldsymbol{x}, t) + K_{\rm tot}(\boldsymbol{x}, t), \tag{5}$$

where

$$K_{\rm tot}(\boldsymbol{x}, t) \approx [1 - C(\boldsymbol{x}, t)][a^{-2}N^{-1} \iint_{\Omega_N} d\boldsymbol{x}' C(\boldsymbol{x} + \boldsymbol{x}', t)]^2. \tag{6}$$

It is the availability of this exact integrodifferential equation (IDE) which will allow the possibility of exact analysis and elucidation of the model behavior for large N.

Specifically, the IDE enables an analysis of the evolution of planar interfaces with normal $\boldsymbol{n}$ separating the populated and vacuum states where $C(\boldsymbol{x}, t) = C(\boldsymbol{x} \cdot \boldsymbol{n} - Vt)$ with $C \to 0\,(C_{\rm act})$ as $\boldsymbol{x} \cdot \boldsymbol{n} \to -\infty\ (+\infty)$. We will focus on the $L \times L$ square neighborhoods and circular neighborhoods of radius R. To this end, we introduce a naturally rescaled spatial variable $u \propto \boldsymbol{x} \cdot \boldsymbol{n}$ and recast Eq. (5) for planar interfaces as

$$\partial/\partial t C(u,t) = -pC(u,t) + [1\text{-}C(u,t)]\left[\int du' K(u') C(u + u', t)\right]^2, \tag{7}$$

TABLE I. $p_{eq}(S)$ versus S from CC simulations (1024×1024 cell with PBC for 10^5 MCS) with strip geometries for indicated Ω_N. Uncertainties from 45 simulations for five different C_t from 0.62 to 0.70. Less reliable results for $N = 4$ with $S = 0$ are omitted (cf. Ref. [13]).

Slope S	$N = 4$ ($r = a$)	$N = 8$ ($\sqrt{5}a$)	$N = 8$ (a, $2a$)	$N = 8$ (a, $\sqrt{2}a$)	$N = 12$ (a, $2a$, $3a$)
0	⋯	0.151 121(2)	0.147 948(13)	0.146 807(3)	0.168 721(12)
1/6	0.080 480(8)	0.151 111(1)	0.147 939(6)	0.146 802(2)	0.168 766(9)
1/5	0.081 151(9)	0.151 109(1)	0.147 957(6)	0.146 808(1)	0.168 771(7)
1/4	0.081 978(8)	0.151 100(1)	0.147 976(7)	0.146 808(1)	0.168 793(8)
1/3	0.082 974(10)	0.151 090(1)	0.148 004(6)	0.146 806(1)	0.168 828(7)
1/2	0.084 134(13)	0.151 070(1)	0.148 086(9)	0.146 807(2)	0.168 899(10)
1	0.084 941(40)	0.151 037(2)	0.148 134(10)	0.146 806(2)	0.169 000(11)

where even $K(u)$ satisfies $\int duK(u) = \int duu^2K(u) = 1$ and $K(u) > 0$ for $-u_s < u < +u_s$. For an $L \times L$ square neighborhood, the vertical interfaces correspond to $u = \sqrt{12}\ x/L$ and $K(u) = 1/\sqrt{12}$ with $u_s = \sqrt{3}$ and diagonal interfaces to $u = \sqrt{12}(x\text{-}y)/L$ and $K(u) = (1\text{-}|u|/\sqrt{6})/\sqrt{6}$ with $u_s = \sqrt{6}$. For a circular neighborhood of radius R, one has that $u = 2x/R$ and $K(u) = \pi^{-1}(1\text{-}u^2/4)^{1/2}$ with $u_s = 2$. Equation (7) has solutions of the form $C(u, t) = C(u\text{-}vt)$, but we focus on the stationary interfaces ($v = V = 0$) corresponding to $p = p_{eq}$. The feature that $K(u)$ depends on the interface orientation and neighborhood shape suggests that the same is true of p_{eq}, i.e., that generic 2PC persists as $N \to \infty$ in the spirit of the Grinstein hypothesis [37]. Remarkably, we show that this is not the case.

It is also instructive to note that numerical analysis of Eq. (7) introduces a periodic spatial grid $u_j = ju_s/M$ and sets $C(u_j, t) = C_j(t)$. Then, a standard composite quadrature rule converts Eq. (7) into the so-called lattice differential equations (LDEs) [42,43]

$$d/dt\, C_j = -pC_j + (1\text{-}C_j)\left[\sum_{-M\le m\le +M} K_m C_{j+m}\right]^2, \quad (8)$$

where $K_m = K(mu_s/M)/K_{\rm sum} = K_{-m}$ for $-M < m < +M$, $K_{\pm M} = \frac{1}{2}K(\pm u_s)/K_{\rm sum}$, and $K_{\rm sum} = \frac{1}{2}K(-u_s) + \sum_{-M<m<+M} K(mu_s/M) + \frac{1}{2}K(+u_s)$. The constraint $\sum_{-M\le m\le +M} K_m = 1$ for any M ensures that Eq. (8) supports concentration profiles with the appropriate asymptotic behavior $C_j \to C_{\rm act}(p)$ as $j \to \infty$.

To analyze the stationary profile solutions, it is convenient to introduce nonanalytic MF-type kinetics $R_{\rm MFN}(C, p) = -2[pC/(1-C)]^{1/2} + 2C$, which has the same steady states as $R_{\rm MF}(C, p)$ in Eq. (2). Then, the time-invariant forms of Eqs. (7) and (8) at $p = p_{eq}$ become

$$\begin{aligned}\Delta^{\circ}C(u) &\equiv 2\int_{0<u'<u_s} du'K(u')[C(u+u') - 2C(u) + C(u-u')] \\ &= -R_{\rm MFN}(C(u), p_{eq}),\end{aligned} \quad (9)$$

where $\Delta^{\circ}C(u)$ can be regarded as a nonlocal second derivative [reducing to $\partial^2/\partial u^2\ C(u)$ in the "diffusion approximation" [36]] and

$$\begin{aligned}\Delta_K C_j &\equiv 2\sum_{+1\le m\le +M} K_m(C_{j+m} - 2C_j + C_{j\text{-}m}) \\ &= -R_{\rm MFN}(C_j, p_{eq}),\end{aligned} \quad (10)$$

where $\Delta_K\ C_j$ constitutes a discrete version of a second derivative. Equations (9) and (10) also prompt consideration of stationary solutions with the appropriate asymptotics for

$$\partial^2/\partial u^2 C(u) = -R_{\rm MFN}(C(u), p_{eq}). \quad (11)$$

Equation (11) can be regarded as the steady-state form of a nonanalytic RDE. Our key point here is to emphasize the similarity in form of all of Eqs. (9)–(11). In all cases, p_{eq} is not known *a priori*.

Complete analysis of the stationary profiles is nontrivial for Eqs. (9) and (10). However, integrating the various types of second derivatives over the profiles gives the difference of the corresponding first derivatives evaluated at $u = \pm\infty$ which vanish. Thus, we conclude that $\int_{-\infty<u<+\infty} R_{\rm MFN}(C_{eq}(u), p_{eq})\ du = 0$ for both Eqs. (9) and (11), and the analogous discrete condition applies for Eq. (10). However, Eqs. (9) and (11) do not have the same stationary profile. Asymptotic analysis reveals an exponential decay $C \to C_{\rm act}$ as u or $j \to \infty$, but the decay rate depends on the form of $K(u)$, i.e., on interface orientation and Ω_N shape for Eq. (9), and it is different for Eq. (11). Similarly, asymptotic decay as u or $j \to -\infty$ where C and $C_j \to 0$ for Eqs. (9) or (10) is smooth and faster than exponential. However, one finds that $C(u) \sim p_{eq}(u - u_0)^4/36$ for $u \ge u_0$, with $C(u) \equiv 0$ for $u \le u_0$ (for finite u_0) for Eq. (11). Thus, while the profiles for Eqs. (9) and (11) are very similar in overall form [Fig. 3(a)], they differ fundamentally in detail. Nonetheless, we show that Eqs. (9)–(11) all share the same p_{eq}.

Although it is not the problem of central interest, it is instructive to now provide a more complete analysis for Eq. (11) after introducing an effective potential

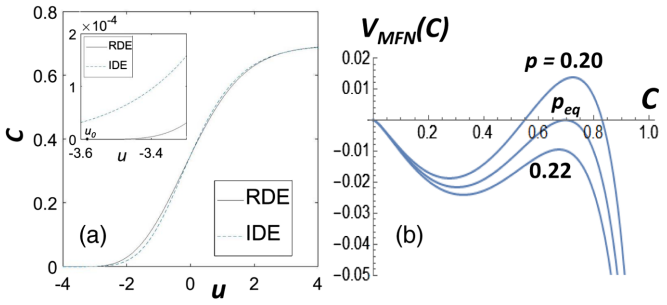

FIG. 3. (a) Stationary profiles at $p = p_{\rm eq}$ for the IDE (9) for constant $K(u)$ and the RDE (11) where $u_0 \approx -3.570\,837\,9$. Profiles have $C(0) = C_{\rm act}/2$. (b) $V_{\rm MFN}(C)$ versus C from Eq. (12) for $p = 0.20$, $p = p_{\rm eq}$(MFN), $p = 0.22$.

$$V_{\rm MFN}(C,p) = \int_{0<C'<C} R_{\rm MFN}(C',p)dC' = 2p^{1/2}[C(1-C)]^{1/2} - p^{1/2}\cos^{-1}(1-2C) + C^2 \tag{12}$$

so that $R_{\rm MFN}(C,p) = \partial/\partial C\, V_{\rm MFN}(C,p)$. Figure 3(b) shows the form of $V_{\rm MFN}(C,p)$. Then, Eq. (11) can be regarded as describing the motion of a pseudoparticle with position C at time u in an external potential $V_{\rm MFN}$. Conservation of energy for this system implies that $E(u) = \frac{1}{2}(\partial C/\partial u)^2 + V_{\rm MFN}(C,p)$ is u independent. For the stationary profile at $p = p_{\rm eq}$, the pseudoparticle starts at the potential maximum at $C = 0$ at time $u = -\infty$ with negligible velocity and moves down the potential landscape reaching and remaining at the other maximum at $C = C_{\rm act}$ only at time $u = +\infty$. This requires equal height potential maxima [see Fig. 3(b)] so that $V_{\rm MFN}(C_{\rm act}, p_{\rm eq}) = 0$ mimicking a Maxwell-type construction balancing the positive and negative areas under $R_{\rm MFC}(C)$ for $0 < C < C_{\rm act}$. This relation implies that

$$(p_{\rm eq})^{1/2}\cos^{-1}[-(1-4p_{\rm eq})^{1/2}] = \tfrac{1}{2} + p_{\rm eq} + \tfrac{1}{2}(1-4p_{\rm eq})^{1/2}, \tag{13}$$

which yields $p_{\rm eq} = p_{\rm eq}(\text{MFN}) = 0.211\,376\,320\,412\,833\,7\ldots$

Analysis of Eqs. (9) and (10) is more challenging given the lack of a direct mapping onto Newtonian dynamics. However, we can embed these time-independent problems into infinite-dimensional dynamical systems incorporating Hamiltonian structure together with dissipation. All of Eqs. (9)–(11) correspond to stationary solutions of dynamical equations

$$\partial^2/\partial t^2 C = -\gamma\partial/\partial t\, C + \Delta^* C - \partial/\partial C\, \tilde{V}_{\rm MFN}(C,p), \tag{14}$$

where $\tilde{V}_{\rm MFN}(C,p) = -V_{\rm MFN}(C,p)$ is a double-well potential, $\gamma > 0$ introduces dissipation, and where $\Delta^* = \Delta^\circ$ for Eq. (9), $\Delta^* = \Delta_K$ for Eq. (10), and $\Delta^* = \partial^2/\partial u^2$ for Eq. (11).

We consider first the discrete case (10). C is replaced by C_j in the LDE (14), which constitutes a dynamical problem involving an infinite elastic chain of pseudoparticles with displacements C_j subject both to an external potential and to damping. We define the total kinetic, elastic, and external potential energies as

$$K = \tfrac{1}{2}\sum_{-\infty<m<+\infty}(d/dtC_m)^2,$$
$$V^{\rm elast} = \sum_{1\le i\le+M}\sum_{-\infty<k<+\infty}\tfrac{1}{2}K_i(C_{k+i}-C_k)^2, \quad \text{and}$$
$$V^{\rm ext}(p) = \sum_{-\infty<m<+\infty}\tilde{V}_{\rm MFN}(C_m,p), \tag{15}$$

respectively. Then, it is straightforward to show that the total system energy $E_{\rm tot} = K + V^{\rm elast} + V^{\rm ext}(p)$ decreases monotonically with increasing time t for $\gamma > 0$.

Thus, the propagating interface solutions of the LDE (14) must move in a direction corresponding to the displacement of the less stable by the more stable steady state, where these correspond to the higher and lower local minimum of $\tilde{V}_{\rm MFN}$, respectively. For $p = p_{\rm eq}$(MFN) where the local minima of $\tilde{V}_{\rm MFN}$ are equal, the interface propagation would be inconsistent with the feature that $E_{\rm tot}$ should be monotonically decreasing. Thus, the LDEs (14) for all $M > 1$ share the same $p_{\rm eq}$ as the continuum RDE [44]. The numerical analysis supports this result.

Since the LDEs recover the IDEs as $M \to \infty$, the IDEs also have the same $p_{\rm eq}$. An alternative argument notes that the IDE (14) describes the dynamics of a continuum elastic material with damping and subject to an external potential. Elastic, external, and kinetic energy functionals can be constructed generating the evolution equation (14) via functional differentiation. Then, the argument used above shows that a stationary solution only exists for $p = p_{\rm eq}$(MFN). In conclusion, the IDE and LDE for all interface orientations and Ω_N shapes, and the RDE, all share the same $p_{\rm eq} = 0.211\,376\,320\,412\,833\,7\ldots$

In summary, we explore a class of Schloegl or contact models with spontaneous particle annihilation and autocatalytic particle creation requiring $n \ge 2$ populated sites in some neighborhood, Ω_N. The models have common MF kinetics. They exhibit a discontinuous transition between populated and vacuum states. Orientation-dependent equistability is found for small Ω_N and might be expected for large Ω_N given the form of the governing IDEs. However, while the interface profiles shape depends on orientation as $N \to \infty$, we find a unique equistability point which is shared by the related LDEs and continuum nonanalytic RDEs (see, also, Ref. [45]). We thus establish a Gibbs phase rule for these nonequilibrium models as $N \to \infty$. This elucidation of nonequilibrium phase transitions, particularly poorly understood generic 2PC behavior, is enabled by a combination of tailored KMC simulation

and exact analytic treatment of the spatiotemporal behavior for $N \to \infty$.

D.-J. L. and J. W. E. were supported by the U.S. Department of Energy–Basic Energy Sciences Division of Chemical Sciences, Geosciences, and Biosciences for development of the analytic theory and the lattice-gas modeling and Kinetic Monte Carlo simulation. Research was performed at the Ames Laboratory, which is operated by Iowa State University under Contract No. DE-AC02-07CH11358. C.-J. W. performed the numerical analysis of the evolution equations for which he was partially supported by the Ministry of Science and Technology of Taiwan Grant No. 105-2115-M-194-011-MY2.

[1] J. Marro and R. Dickman, *Nonequilibrium Phase Transitions in Lattice Models* (Cambridge University Press, Cambridge, England, 1999).
[2] G. Odor, Rev. Mod. Phys. **76**, 663 (2004).
[3] M. Henkel, H. Hinrichsen, and S. Luebeck, *Non-Equilibrium Phase Transitions* (Springer, Berlin, 2008), Vol. 1.
[4] H. Hinrichsen, Adv. Phys. **49**, 815 (2000).
[5] "Directing matter and energy: Five challenges for science and the imagination," 2007 USDOE BESAC Report, J. Hemminger (Chair), G. Fleming and M. Ratner (co-Chairs), https://science.energy.gov/~/media/bes/pdf/reports/files/Directing_Matter_and_Energy_rpt.pdf.
[6] J. D. Gunton, M. San Miguel, and P. S. Sahni, in *Phase Transitions and Critical Phenomena*, edited by J. L. Lebowitz and C. Domb (Academic Press, London, 1983).
[7] R. M. Ziff, E. Gulari, and Y. Barshad, Phys. Rev. Lett. **56**, 2553 (1986).
[8] J. W. Evans, D.-J. Liu, and M. Tammaro, Chaos **12**, 131 (2002).
[9] A. L. Toom in *Multicomponent Random Systems*, edited by R. L. Dobrushin and Y. G. Sinai (Dekker, New York, 1980).
[10] C. H. Bennett and G. Grinstein, Phys. Rev. Lett. **55**, 657 (1985).
[11] Y. He, C. Jayaprakash, and G. Grinstein, Phys. Rev. A **42**, 3348 (1990).
[12] M. A. Munoz, F. de los Santos, and M. M. T. da Gama, Eur. Phys. J. B **43**, 73 (2005).
[13] D.-J. Liu, X. Guo, and J. W. Evans, Phys. Rev. Lett. **98**, 050601 (2007).
[14] C.-J. Wang, D.-J. Liu, and J. W. Evans, J. Chem. Phys. **142**, 164105 (2015).
[15] M. Aizenman and J. L. Lebowitz, J. Phys. A **21**, 3801 (1988).
[16] P. I. Hurtado, J. Marro, and P. L. Garrido, Phys. Rev. E **74**, 050101R (2006).
[17] X. Guo, D.-J. Liu, and J. W. Evans, J. Chem. Phys. **130**, 074106 (2009).
[18] J. Gravner, A. E. Holroyd, and R. Morris, Probab. Theory Relat. Fields **153**, 1 (2012).
[19] I. Prigogine and G. Nicolis, *Self-Organization in Non-Equilibrium Systems: From Dissipative Structures to Order through Fluctuations* (Wiley-Blackwell, London, 1977).
[20] A. S. Mikhailov, *Foundations of Synergetics I: Distributed Active Systems*, 2nd ed. (Springer Verlag, Berlin, 1994).
[21] F. Schloegl, Z. Phys. **253**, 147 (1972).
[22] P. Grassberger, Z. Phys. B **47**, 365 (1982).
[23] A. Lawniczak, D. Dab, R. Kapral, and J.-P. Boon, Physica (Amsterdam) **47D**, 132 (1991).
[24] Y. De Decker, G. A. Tsekouras, A. Provata, T. Erneux, and G. Nicolis, Phys. Rev. E **69**, 036203 (2004).
[25] R. Durrett, SIAM Rev. **41**, 677 (1999).
[26] S. Handjani, J. Theor. Probab. **10**, 737 (1997).
[27] L. R. G. Fontes and R. H. Schonmann, Probab. Theory Relat. Fields **141**, 513 (2008).
[28] T. Montford and R. H. Schonmann, Ann. Probab. **37**, 1483 (2009).
[29] S. Chatterjee and R. Durrett, Stoch. Proc. Appl. **123**, 561 (2013).
[30] E. F. da Silva and M. J. de Oliveira, J. Phys. A **44**, 135002 (2011).
[31] E. F. da Silva and M. J. de Oliveira, Comput. Phys. Commun. **183**, 2001 (2012).
[32] M. Biskup, L. Chayes, and N. Crawford, J. Stat. Phys. **122**, 1139 (2006).
[33] E. Luijten, H. W. J. Blöte, and K. Binder, Phys. Rev. E **54**, 4626 (1996).
[34] C.-H. Chan and P. A. Rikvold, Phys. Rev. E **91**, 012103 (2015).
[35] C.-H. Chan and P. A. Rikvold, Phys. Procedia **68**, 20 (2015).
[36] D. Mollison, J. R. Stat. Soc. Ser. B Methodol. **39**, 283 (1977), http://www.jstor.org/stable/2985089.
[37] A non-equilibrium continuum Langevin version of a TDGL model was constructed in Ref. [11] to incorporate spatially asymmetric rules analogous to those of the discrete Toom's model. This continuum model was shown to exhibit generic 2PC.
[38] X. Guo, J. W. Evans, and D.-J. Liu, Physica (Amsterdam) **387A**, 177 (2008).
[39] C.-J. Wang, D.-J. Liu, and J. W. Evans, Phys. Rev. E **85**, 041109 (2012).
[40] R. M. Ziff and B. J. Brosilow, Phys. Rev. A **46**, 4630 (1992).
[41] T. Tome and M. J. de Oliveira, Phys. Rev. Lett. **86**, 5643 (2001).
[42] J. P. Keener, SIAM J. Appl. Math. **47**, 556 (1987).
[43] S.-N. Chow, J. Mallet-Paret, and E. S. Van Vleck, Int. J. Bifurcation Chaos Appl. Sci. Eng. **06**, 1605 (1996).
[44] Contrasting Refs. [38,39], for $M = 1$, we find weak propagation failure anomalies which are familiar for the LDE [42,43].
[45] T. Hillen, SIAM Rev. **49**, 35 (2007).